Supplementary Information (SI) for Journal of Materials Chemistry A.
This journal is © The Royal Society of Chemistry 2024

SUPPLEMENTARY INFORMATION

Dipeptide-Functionalized Type II Heterojunctions: A Bioinspired Dual Functionality for Quinalphos Detection and Photodegradation

Divya,[a] Sanchit Kalra,[a] Sanjeev Saini,[b] Navneet Kaur*[a] and Narinder Singh*[c]

[a] *Department of Chemistry & Centre for Advanced Studies in Chemistry, Panjab University, Chandigarh 160014, India*

[b] *Department of Chemistry, School of Physical Science, DIT University, Dehradun, Uttarakhand, 248009, India*

[c] *Department of Chemistry, Indian Institute of Technology Ropar, Rupnagar, Punjab 140001, India*

Author Information

CORRESPONDING AUTHORS

Navneet Kaur- Department of Chemistry & Centre for Advanced Studies in Chemistry, Panjab University, Chandigarh 160014, India

Email- navneetkaur@pu.ac.in

Narinder Singh-Department of Chemistry, Indian Institute of Technology Ropar, Rupnagar, Punjab 140001, India

Email- nsingh@iitrpr.ac.in

TABLE OF CONTENTS

Sr. No.	Title
	• Materials and reagents • Synthesis of **DM2** • Synthesis and characterization of dipeptide receptor, **DM2** • Fabrication of **DM2**-capped zincoxide nanoparticles(**DM2-capped ZnO NPs**) • Photophysical and electrochemical studies of **DM2**and **DM2-capped ZnO NPs** • Secondary studies of **DM2-capped ZnO NPs** • Cell culture and cytotoxicity analysis
Fig. S1	FT-IR spectrum of **DM2**.
Fig. S2	^{1}H-NMR spectrum of **DM2**.
Fig. S3	^{13}C-NMR spectrum of **DM2**.
Fig. S4	ESI-MS spectrum of **DM2**.
Fig. S5	DLS spectrum of (A) bare ZnO, (B) **DM2-capped ZnO NPs**, (C) FT-IR spectra of DM2 and **DM2-capped ZnO NPs**.
Fig. S6	Full region XPS survey of (A) **DM2** and (B) **DM2-capped ZnO NPs;** High-resolution deconvoluted XPS spectrum of (C) C, 1s; (D) N, 1s; (E) O, 1s; (F) F, 1s of **DM2**.
Fig. S7	(A)Radar plot showing the stability of **DM2-capped ZnO NPs** in terms of fluorescence intensity over 9 days, (B) Time-resolved fluorescence spectrum and (C) TGA plots of bare ZnO and **DM2-capped ZnO NPs**, (D) BET isotherms and (E) BJH plot of **DM2-capped ZnO NPs** and(F) Nyquist plots of GCE, **DM2**, and **DM2-capped ZnO NPs** in 0.1 M KCl containing $[Fe(CN)_6]^{3-/4-}$.
Fig. S8	Changes in the(A)Absorbance, (B) Fluorescence intensity, and (C) Cyclic voltammograms of **DM2**and **DM2-capped ZnO NPs.**
Fig. S9	Changes in the (A) fluorescence intensity of **DM2**upon adding OPPsand (B) Binding studies of **DM2** with OPPs in a bar graph.
Fig. S10	(A, B) Binding studies of **DM2-capped ZnO NPs** upon adding various 1

	mM solutions of OPPs in terms of changes in their FL intensity. (C) Changes in the FL intensity of **DM2-capped ZnO NPs** upon the successive addition of quinalphos. (D) Linear calibration plot between the FL intensity and concentration of quinalphos added.
Fig. S11	Competitive binding studies of **DM2-capped ZnO NPs+quinalphos** in the presence of other tested OPPs.
Fig. S12	Changes in the FL intensity of **DM2-capped ZnO NPs** upon adding 1 mM HCl and 1 mM NaOH solutions in the pH range of 3-11.2.
Fig. S13	Changes in the FL intensity of **DM2-capped ZnO NPs** upon the addition of TBA ClO_4^-.
Fig. S14	Salt perturbation studies of **DM2-capped ZnO NPs+quinalphos**upon the successive addition of TBA ClO_4^-.
Fig. S15	Response time studies of **DM2-capped ZnO NPs** for quinalphos at various time intervals with varying concentrations of quinalphos (A- 35 nM, B- 70 nM, and C-105 nM).
Fig. S16	(A) LSV and (B) DPV plots of **DM2-capped ZnO NPs** upon the successive addition of quinalphos.
Fig. S17	Shifts in the stacked ^{1}H-NMR spectrum of **DM2-capped ZnO NPs** upon the addition of quinalphos *i.e.,* **DM2-capped ZnO NPs+quinalphos** (0.5 eq.) and **DM2-capped ZnO NPs+quinalphos** (1 eq.).
Fig. S18	ESI-MS spectrum of **DM2-capped ZnO NPs+quinalphos** leading to the formation of hydrolyzed product.
Scheme S1	An efficient route for the detection of quinalphos upon its interaction with **DM2-capped ZnO NPs**.
Fig. S19	ESI-MS spectrum of **DM2-capped ZnO NPs+quinalphos** leading to the oxidation of quinalphos, complementing the interaction of **DM2-capped ZnO NPs** with quinalphos.
Fig. S20	Photodegradation of quinalphos by **DM2-capped ZnO NPs**. (A) % Degradation of quinalphos and (B) ln (A/A_0) versus time plot showing the pseudo-first-order kinetics; (C) Degradation efficiency of **DM2-capped ZnO NPs** towards the degradation of quinalphos, azinphos-methyl (AZM), phosmet, chlorpyrifos, malathion, profenofos, diethyl cyanophosphate (DCNP), and diethyl chlorophosphate (DCP).

Fig. S21	Radical scavenging experiment.
Fig. S22	ESI-MS spectrum of **DM2-capped ZnO NPs+quinalphos**validating its transformation into *quinoxaline-2-thiol* (m/z=162).
Fig. S23	ESI-MS spectrum of **DM2-capped ZnO NPs+quinalphos**confirming its conversion into *O-ethyl O-({[2-hydroxyamino) phenyl] amino) methyl} hydrogen phosphonothioate* (m/z=290).
Fig. S24	ESI-MS spectrum showing the absence of peak corresponding to m/z=298 (quinalphos) upon its interaction with **DM2-capped ZnO NPs**.
Fig. S25	DLS spectra of QuinoClean (aerospray comprising of 1:1 solution of oleic acid: vegetable oil) showing its stability over 6 weeks at ambient temperature.
Fig. S26	DLS spectra of 2:1 (oleic acid: vegetable oil) solution for 11 days.
Table S1	Comparison of varying amounts of oleic acid and vegetable oil and their corresponding hydrodynamic size.
Fig. S27	Changes in the (A, C, E, G) absorbance and (B, D, F, H) FL intensity of **DM2-capped ZnO NPs**-based core@corona formulation (A, B) over 6 weeks; (C, D) upon the addition of 1 mM HCl and 1mM NaOH respectively; (E, F) upon addition of TBA ClO_4^- and (G, H) effect of temperature variation.
Table S2	Comparison table of present work with other analytical techniques.

Materials and reagents: The chemicals employed for the synthesis of dipeptide *i.e.,* benzyl ester of phenylalanine, N-tertbutyloxycarbonyl leucine (N-Boc-Leu), *N, N*-diisopropylethylamine (DIPEA), 1-ethyl-*3-(3-dimethylaminopropyl) carbodiimide* (EDC), hydroxybenzotriazole (HOBt), 1-fluoro-2-isocyanatobenzene, trifluoroacetic acid (TFA), dichloromethane (DCM) and oleic acid were purchased from TCI Chemical limited. The pesticide solutions were procured from Sigma-Aldrich and their 1 mM solutions were prepared in Milli-Q water. Zinc nitrate hexahydrate [Zn $(NO_3)_2.6H_2O$] was purchased from

Sigma-Aldrich. These chemicals were employed in the studies without any further purification.

Synthesis of DM2: The synthesis of DM2was carried out in a stepwise manner. Initially, (A) was synthesized by a coupling reaction between the benzyl ester of phenylalanine (1.2 *eq.*) and *N*-Boc-Leu (1 *eq.*) at 0-4ºC under an inert atmosphere using DIPEA (2.2 *eq.*) as a base in the presence of coupling agent, EDC (1.2 *eq.*) and HOBt (1.2 *eq.*). The reaction was quenched with ice-cold Milli-Q water and concentrated under reduced pressure resulting in pure product (A). It was refluxed in TFA/DCM (20%) to accomplish the deprotection of Boc group leading to the formation of precursor (B).The reaction of precursor (B) with 1-fluoro-2-isocyanatobenzene in acetonitrile at room temperature resulted in the formation of dipeptide *i.e., N*-functionalized naphthyl urea derivative of dipeptide (DM2)as shown in Scheme 1. FT-IR, ^{1}H-NMR, ^{13}C-NMR, and ESI-MS techniques confirmed the formation of *benzyl((2-fluorophenyl) carbamoyl)-L-leucyl-Lphenylalaninate*, DM2 as shown inFig. S1-S4. The characteristic carbonyl stretching frequency of -CO-NH- moiety of peptide bond appeared at 1638 cm^{-1} in the FT-IR spectrum of DM2. The ^{1}H-NMR and ^{13}C-NMR established the formation of DM2 and its ESI-MS spectrum displayed an M+1 peak at m/z=506 confirming the formation of dipeptide, DM2.

Characterization data of *Benzyl((2-fluorophenyl) carbamoyl)-L-leucyl-L-phenylalaninate* [DM2]:^{1}H-NMR (400 MHz, DMSO-d_6) δ 8.54 (d, J = 7.3 Hz, 1H), 8.36 (d, J = 3.1 Hz, 1H), 8.11 – 8.06 (m, 1H), 7.37 – 6.98 (m, 12H), 6.88 (q, J = 7.6 Hz, 1H), 6.79 (d, J = 8.5 Hz, 1H), 5.07 – 4.97 (m, 2H), 4.54 – 4.44 (m, 1H), 4.30 – 4.19 (m, 1H), 3.09 – 2.87 (m, 2H), 1.53 (q, J = 7.6, 6.1 Hz, 1H), 1.41 – 1.18 (m, 2H), 0.81 (d, J = 6.7 Hz, 6H); **^{13}C-NMR** (DMSO-d_6) δ 173.24, 171.71, 154.80, 137.70, 136.25, 129.63, 128.86, 128.73, 128.53, 128.40, 127.01, 124.86, 122.06, 120.53, 115.38, 115.19, 66.54, 54.15, 51.48, 42.61, 36.96, 24.66, 23.53, 22.42; **ESI-MS**: (TOF MS ES^{+}) m/z: [M+H] = 506.

Fabrication of DM2-capped ZnO NPs: A cost-effective and straightforward sol-gel route was adopted for the fabrication of DM2-capped ZnO NPs. Typically, 3 mmol zinc nitrate hexahydrate and 2 mmol DM2 were dissolved in 5 mL anhydrous ethanol followed by stirring at ambient temperature. Parallel to this, a 3 mmol alcoholic NaOH solution (precipitating agent) was prepared in ethanol. Further, a few drops of NaOH solution were poured into the Zn^{2+} precursor solution until pH was adjusted to 8-9. The stirring was continued for another 2 h and a homogenous suspension was obtained. This resulted in a tailored structure of dipeptide-capped zinc oxide nanoparticles which were separated by ultracentrifugation. It was further treated several times with ethanol and water to ensure the extermination of undesirable impurities. The collected homogenous white precipitates were dried in a hot air oven for 3 h at 50ºC. The as-prepared nanohybrid material was denoted as dipeptide-capped ZnO nanoparticles, DM2-capped ZnO NPs.

Photophysical and electrochemical studies of DM2 and DM2-capped ZnO NPs: The recognition studies of DM2 and DM2-capped ZnO NPs had been executed using 1 mM solutions of OPPs *viz.* diethyl cyanophosphate, diethyl chlorophosphate, phosmet, malathion, azinphos methyl, chlorpyrifos, profenofos, and quinalphos. The photophysical studies of DM2 were carried out by using a 0.2 mM solution of ligand DM2 in DMF owing to its excellent solubility in this aprotic solvent. It displayed an absorbance at λ273 nm ascribed to $\pi \rightarrow \pi^*$ transitions. The photophysical studies of DM2 were performed on a fluorescence spectrophotometer at room temperature. The binding studies were carried out by employing an excitation wavelength of 273 nm and the emission wavelength appeared at 321 nm. Further, the binding studies were performed using the 1 mM solutions of various OPPs (in water). The emission profiles were noted upon the addition of OPPs into volumetric flasks containing a 5 mL solution of DM2 as shown in Fig. S9. It was found that DM2 did not show a selective response towards any tested OPPs. Later, an organic-inorganic nanohybrid

material (DM2-capped ZnO NPs) was fabricated to characterize and explore the capping-related spectroscopic and electrochemical properties of DM2 capped over the surface of ZnO. The practical utility of the developed material, DM2-capped ZnO NPs was established by performing various secondary studies such as the effect of pH, salt perturbation, interference studies, response time studies, *etc.* The effect of acidic and basic pH was established using freshly prepared 1 mM HCl and 1 mM NaOH solutions respectively. Salt studies were performed by adding tertiary butyl ammonium perchlorate to a solution of DM2-capped ZnO NPs until the saturation point. For interference studies, 2-fold concentrations of tested OPPs were added to the complex of DM2-capped ZnO NPs+quinalphos. The response time studies of DM2-capped ZnO NPs for quinalphos were examined by noting its fluorescence profiles up to 140 s with varying concentrations of quinalphos (35, 70, and 105 nM). The cyclic voltammetry of DM2-capped ZnO NPs was performed using a glassy carbon electrode (GCE), Ag/AgCl, and platinum wire as the working electrode, reference electrode, and auxiliary/counter electrode respectively using 0.1 M PBS buffer (pH=7.4) as electrolyte medium and cyclic voltammograms were obtained in the -1.5 V to +1.5 V potential range at a scan rate of 100 mV/s. The scan rate studies were accomplished in the potential range of 10-250 mV/s. Before the onset of every experiment, the surface of the working electrode was prepared by polishing it with alumina slurry and washed thrice with ethanol and Milli-Q water. The reference electrode was filled with 3 M KCl solution before the onset of every experiment. The impedance studies were performed by employing 0.1 M KCl containing $[Fe(CN)_6]^{3-/4-}$ in the 10^6-0.001 Hz frequency range at open circuit voltage possessing a current amplitude of 5 mV. The current *vs.* time *i.e.,* amperometry titrations were performed in 0.01 M PBS buffer at a potential of +0.39 V and -0.39 V having a time duration of 0.01 s and a time interval of 60 s.

Secondary studies of DM2-capped ZnO NPs: The effect of pH was explored by adding 1 mM HCl and 1 mM NaOH solutions to DM2-capped ZnO NPs and the pH of the solution was varied from 3-11.5. Their FL intensity revealed that the material showed a stable response in varying pH ranges as shown in Fig. S12. A minimal salt effect was observed upon the gradual addition of TBA ClO_4^- to DM2-capped ZnO NPs as there were negligible changes in the FL intensity of DM2-capped ZnO NPs upon its addition up to 120 *eq.* as shown in Fig. S13. The effect of salt was also analyzed after the binding of quinalphos to DM2-capped ZnO NPs and interestingly, the complex showed a stable salt response as shown in Fig. S14. The ability of quinalphos to bind with DM2-capped ZnO NPs was also explored with time in the presence of varying concentrations of DM2-capped ZnO NPs+quinalphos. It was perceived that the quinalphos could bind with DM2-capped ZnO NPs within the first 20 s and the response remained unchanged up to 140 s as shown in Fig. S15. It could be concluded that the proposed material served well towards the selective recognition of quinalphos under given experimental conditions.

Cell culture and cytotoxicity analysis: The L929 fibroblast cell lines were procured from the National Chemical Laboratory, Pune. The cells were grown in 10% fetal bovine serum and 1% penicillin-streptomycin antibiotic solution in DMEM (Dulbecco's Modified Eagle Medium) media at 37ºC and a 5% CO_2 humidified atmosphere. The cells were allowed to grow for 1-2 days before their analysis until their 80% growth was obtained. The grown cells were further stored in an incubator at 37ºC and a 5% CO_2 humidified atmosphere. The suspension thus obtained was centrifuged at 2000 rpm for 2 min to result in the precipitation of cells. Later, the cells were rinsed thoroughly with trypsin and resuspended in DMEM. On average, 10,000 cells were spread and allowed to grow onto a culture plate before DM2-capped ZnO NPs tagging with varying concentrations (0.1, 0.2, 1, 2, 4 μg).

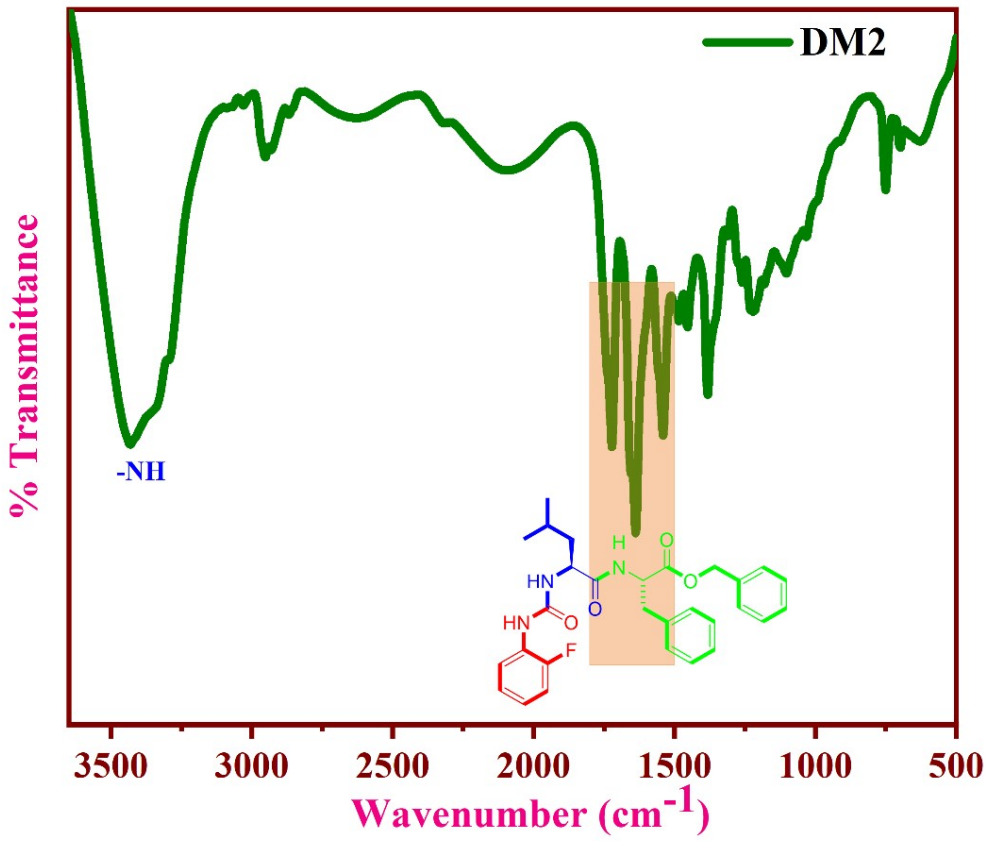

Fig. S1: FT-IR spectrum of **DM2**.

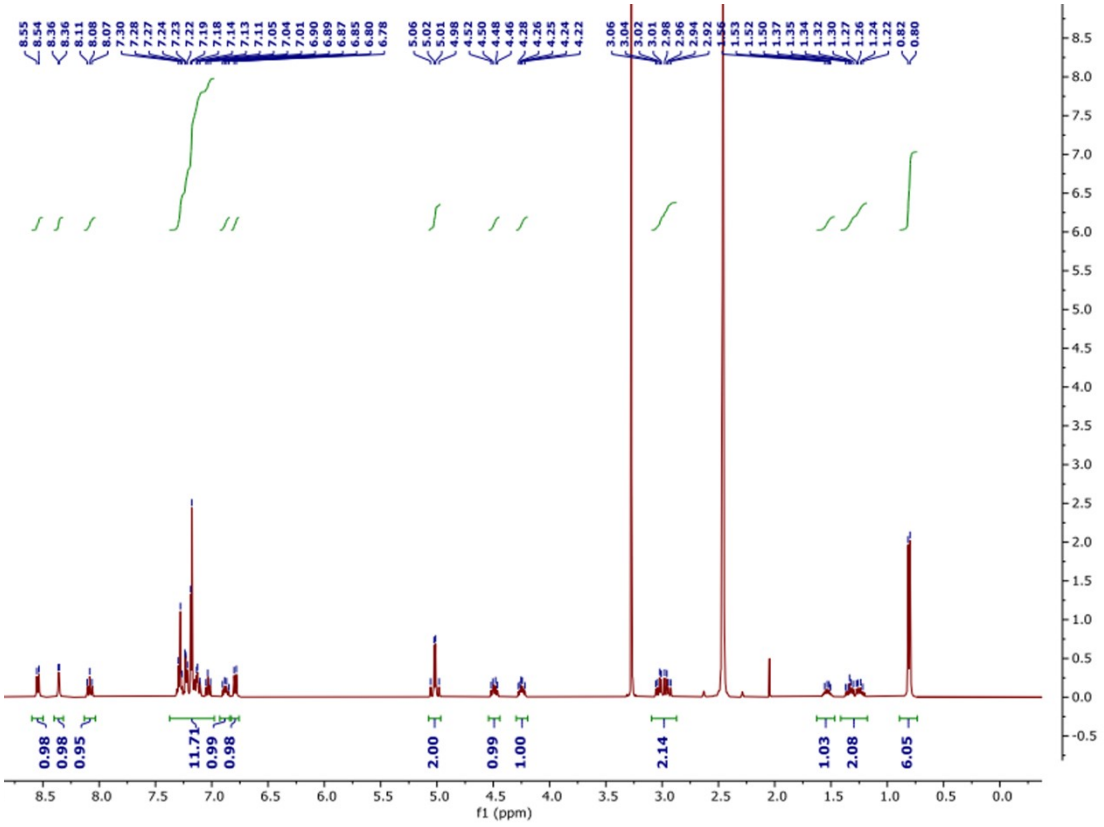

Fig. S2: ^{1}H-NMR spectrum of **DM2**.

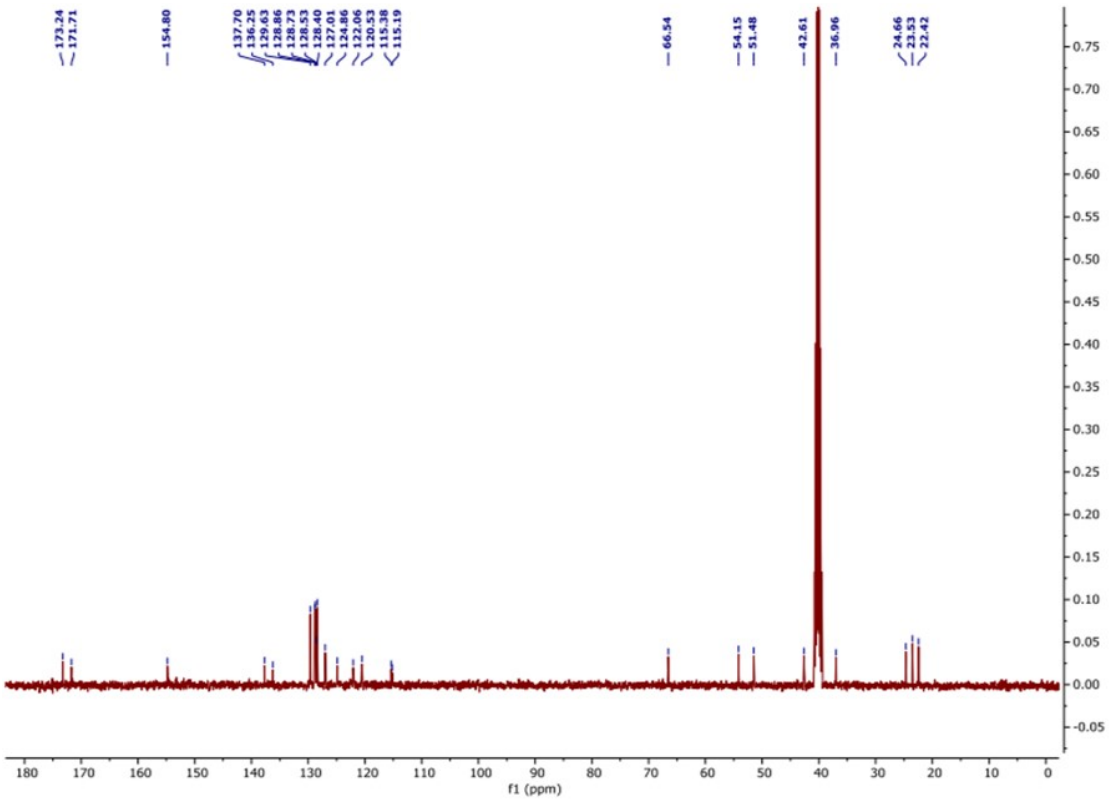

Fig. S3: ^{13}C-NMR spectrum of **DM2**.

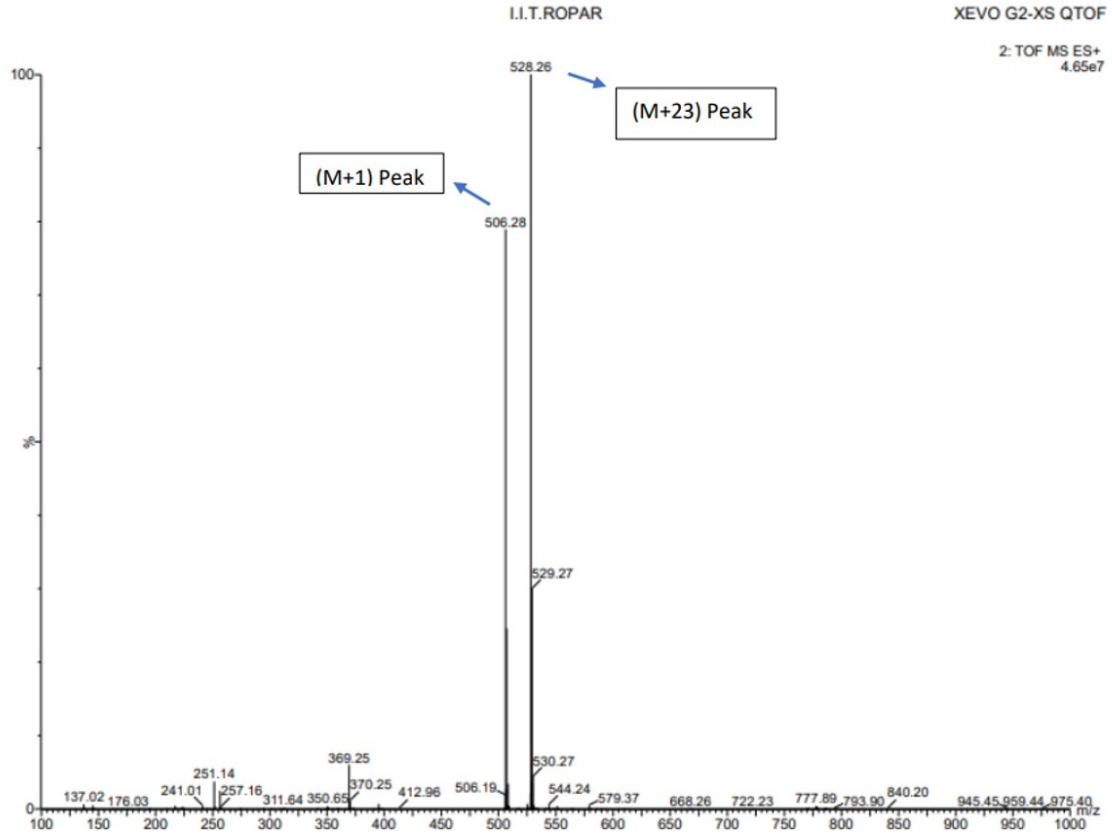

Fig. S4: ESI-MS spectrum of **DM2**.

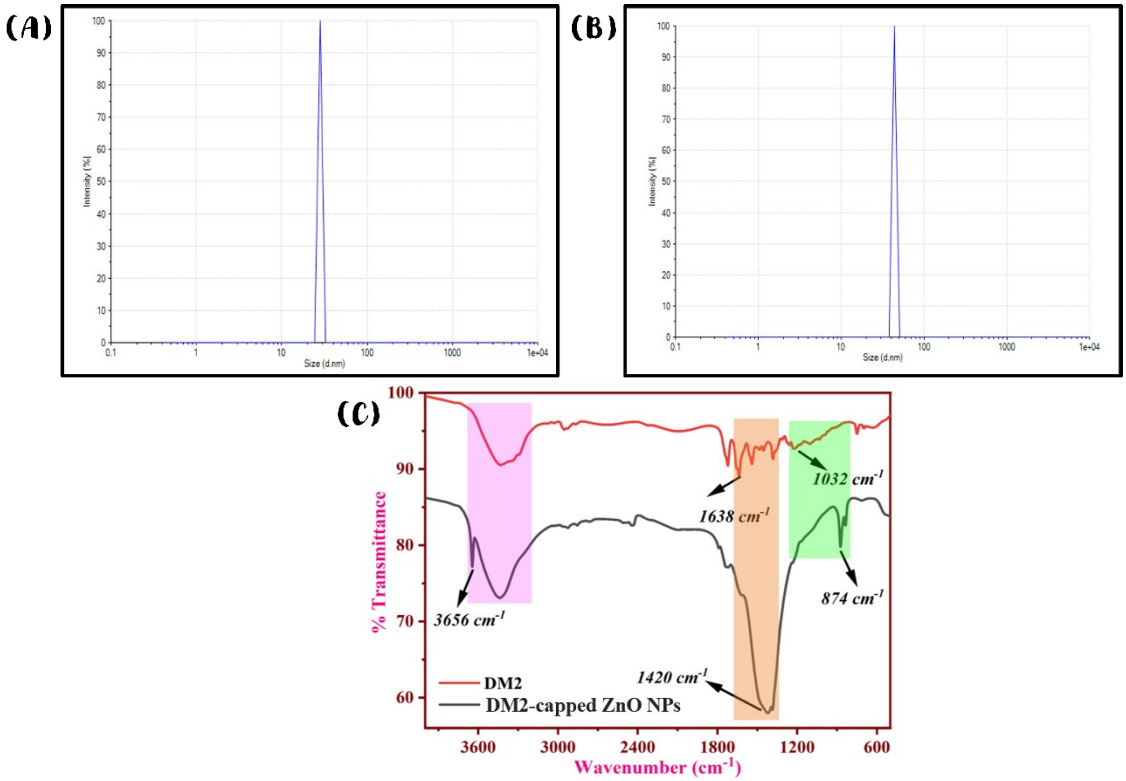

Fig. S5: DLS spectrum of (A) bare ZnO, (B) **DM2-capped ZnO NPs**, (C) FT-IR spectra of **DM2** and **DM2-capped ZnO NPs**.

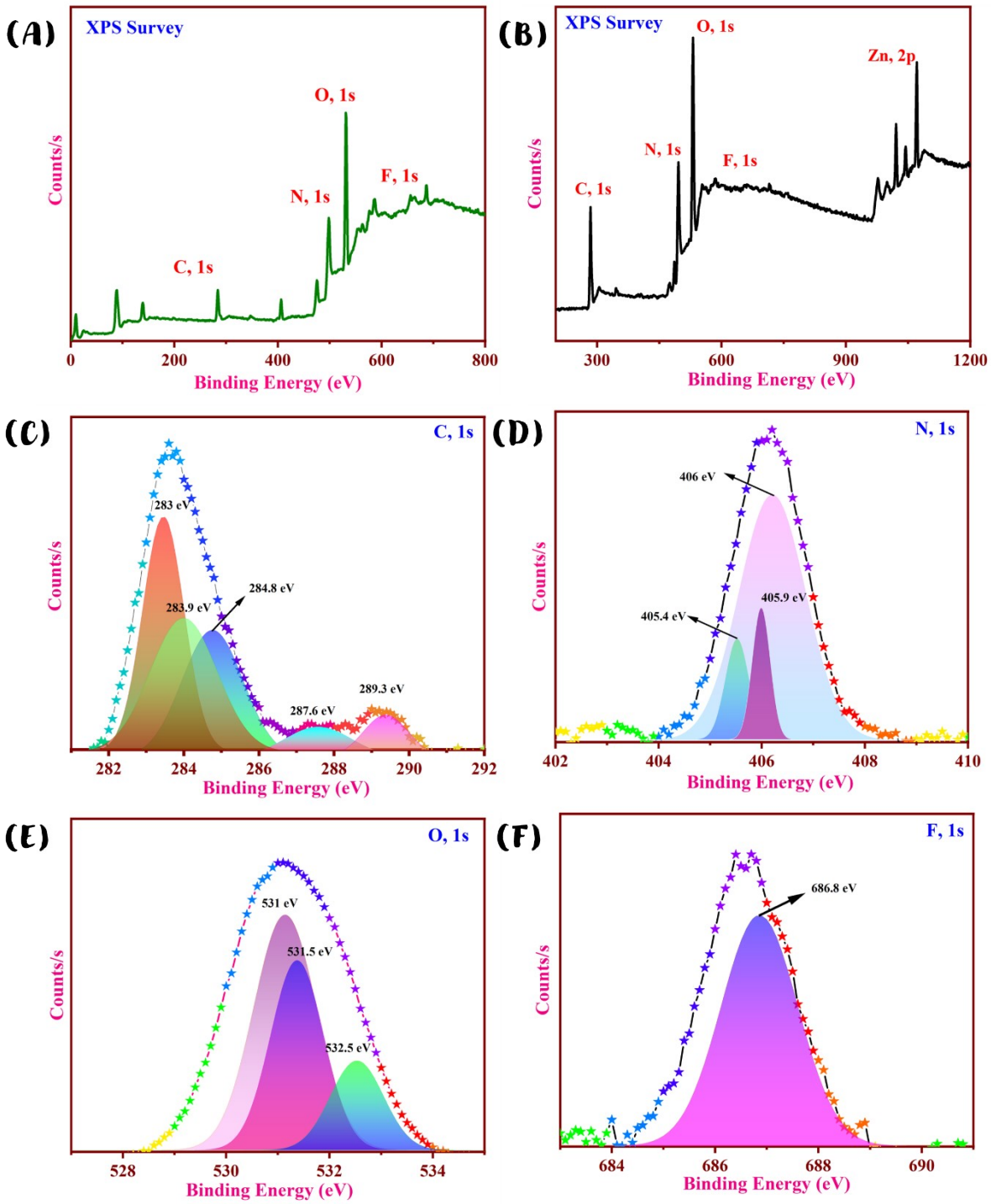

Fig. S6: Full region XPS survey of (A) **DM2** and (B) **DM2-capped ZnO NPs;**High-resolution deconvoluted XPS spectrum of (C) C, 1s; (D) N, 1s; (E) O, 1s; (F) F, 1s of **DM2**.

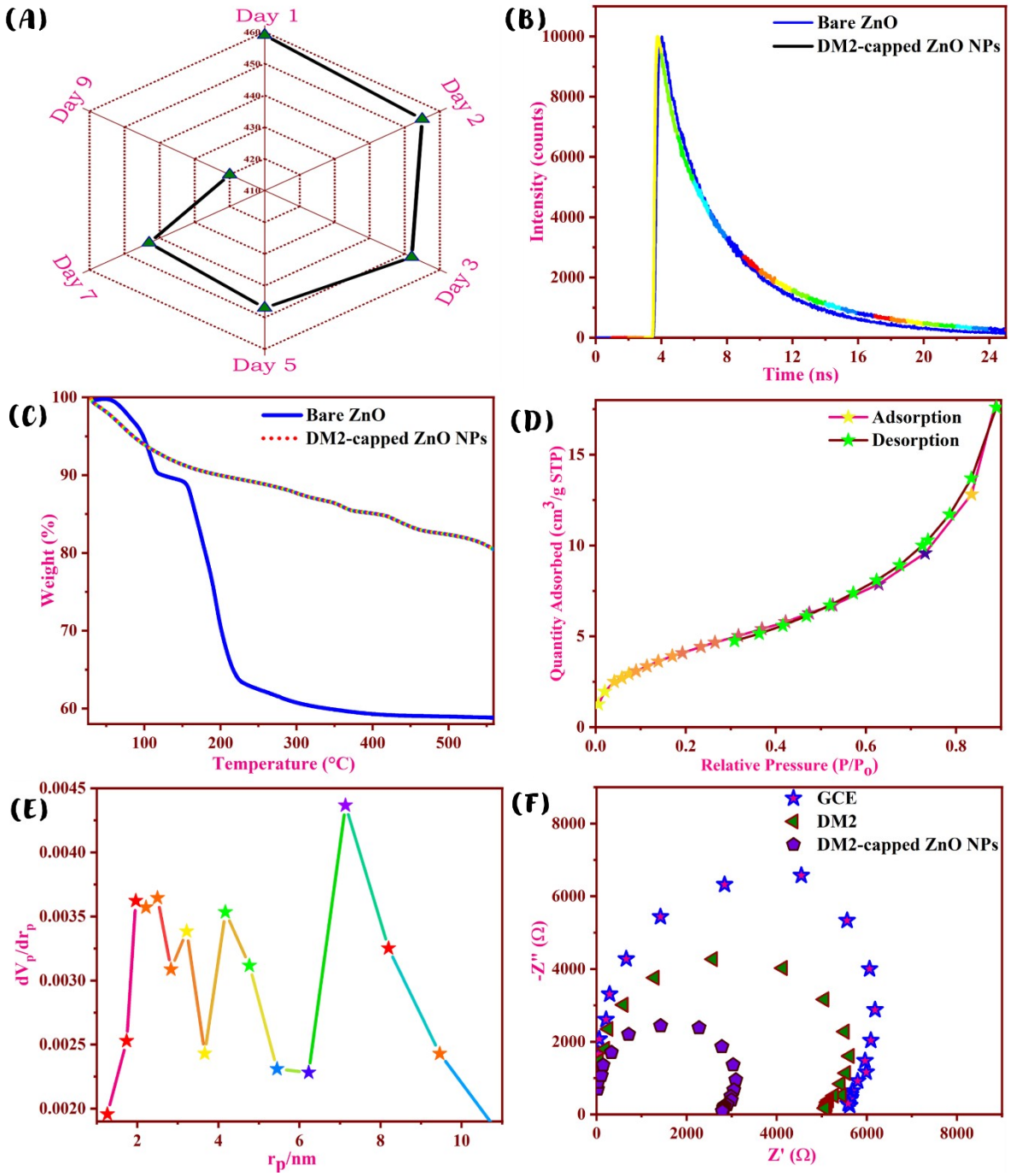

Fig. S7: (A)Radar plot showing the stability of **DM2-capped ZnO NPs** in terms of fluorescence intensity over 9 days, (B) Time-resolved fluorescence spectrum and (C) TGA plots of bare ZnO and **DM2-capped ZnO NPs**, (D) BET isotherms and (E) BJH plot of **DM2-capped ZnO NPs** and(F) Nyquist plots of GCE, **DM2**, and **DM2-capped ZnO NPs** in 0.1 M KCl containing $[Fe(CN)_6]^{3-/4-}$.

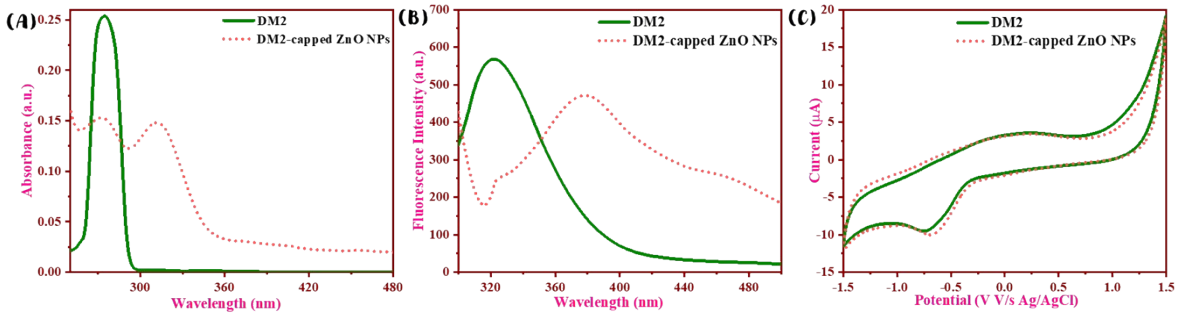

Fig. S8: Changes in the(A)Absorbance, (B) Fluorescence intensity, and (C) Cyclic voltammograms of **DM2** and **DM2-capped ZnO NPs**.

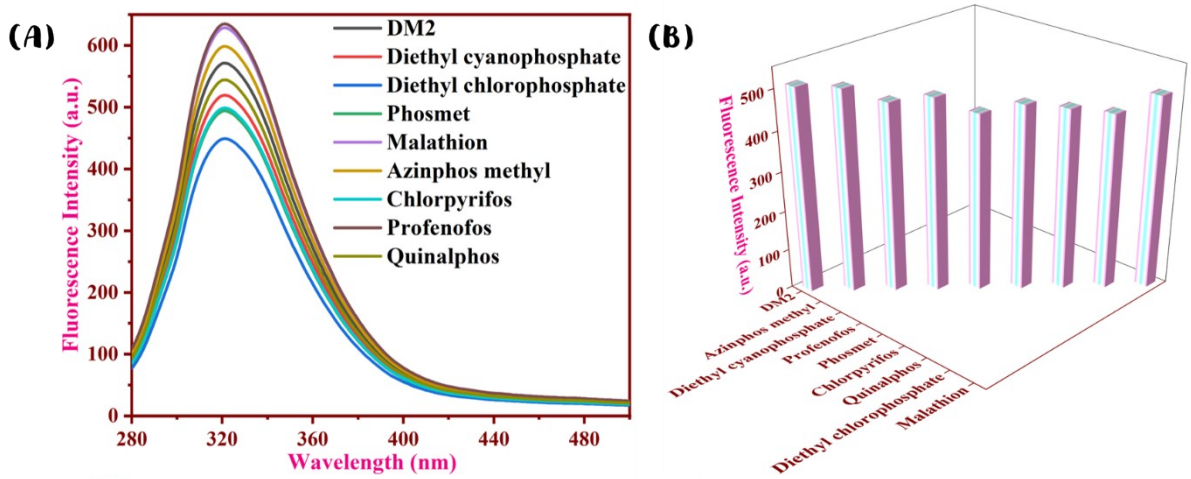

Fig. S9: Changes in the (A) fluorescence intensity of **DM2**upon adding OPPsand (B) Binding studies of **DM2** with OPPs in a bar graph.

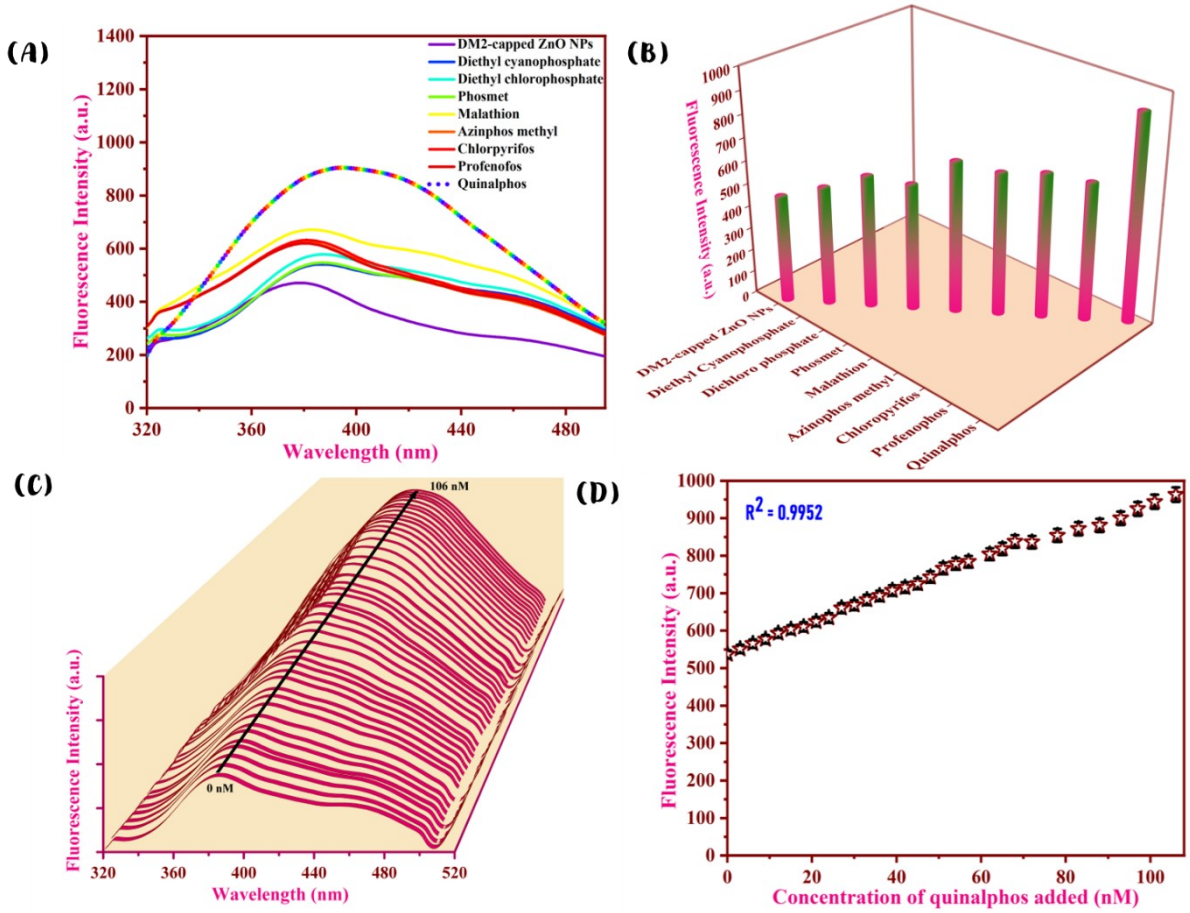

Fig.S10: (A, B) Binding studies of **DM2-capped ZnO NPs** upon adding various 1 mM solutions of OPPs in terms of changes in their FL intensity. (C) Changes in the FL intensity of **DM2-capped ZnO NPs** upon the successive addition of quinalphos. (D) Linear calibration plot between the FL intensity and concentration of quinalphos added.

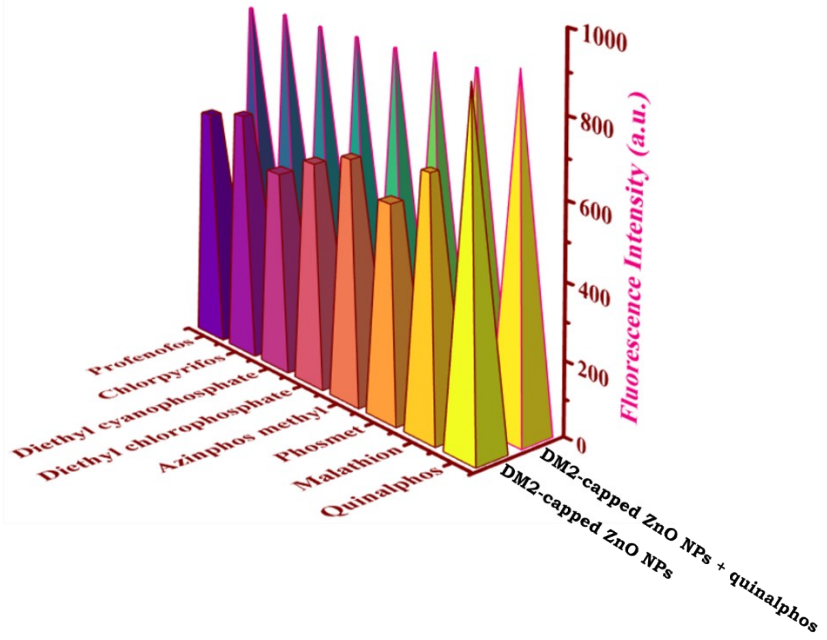

Fig. S11: Competitive binding studies of **DM2-capped ZnO NPs+quinalphos** in the presence of other tested OPPs.

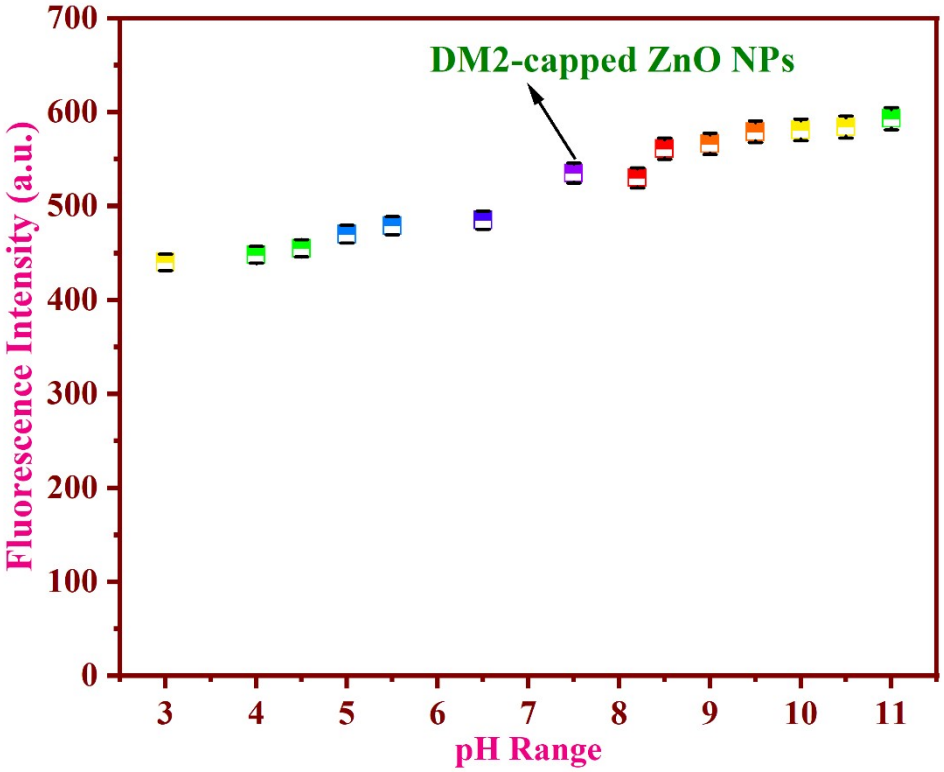

Fig. S12: Changes in the FL intensity of **DM2-capped ZnO NPs** upon adding 1 mM HCl and 1 mM NaOH solutions in the pH range of 3-11.2.

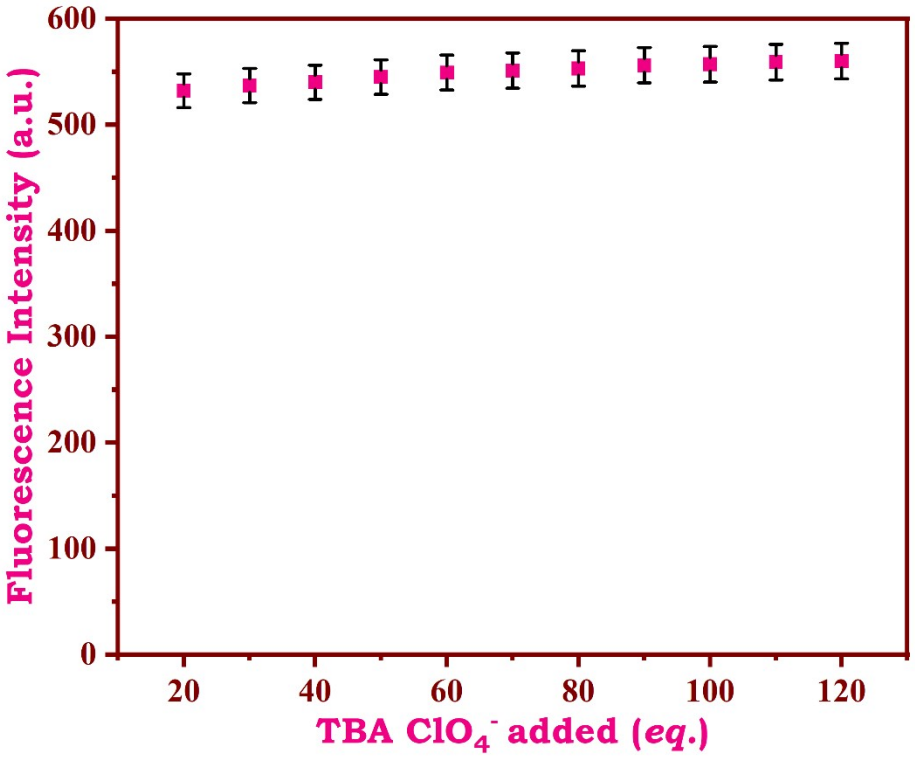

Fig. S13: Changes in the FL intensity of **DM2-capped ZnO NPs** upon the addition of TBA ClO_4^-.

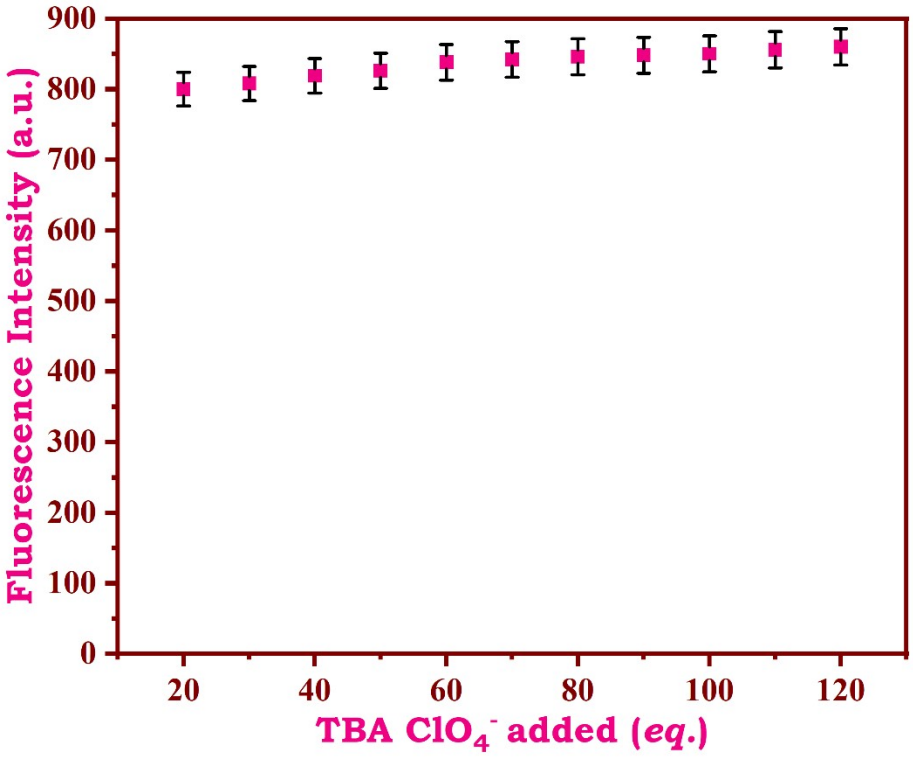

Fig. S14: Salt perturbation studies of **DM2-capped ZnO NPs+quinalphos** upon the successive addition of TBA ClO_4^-.

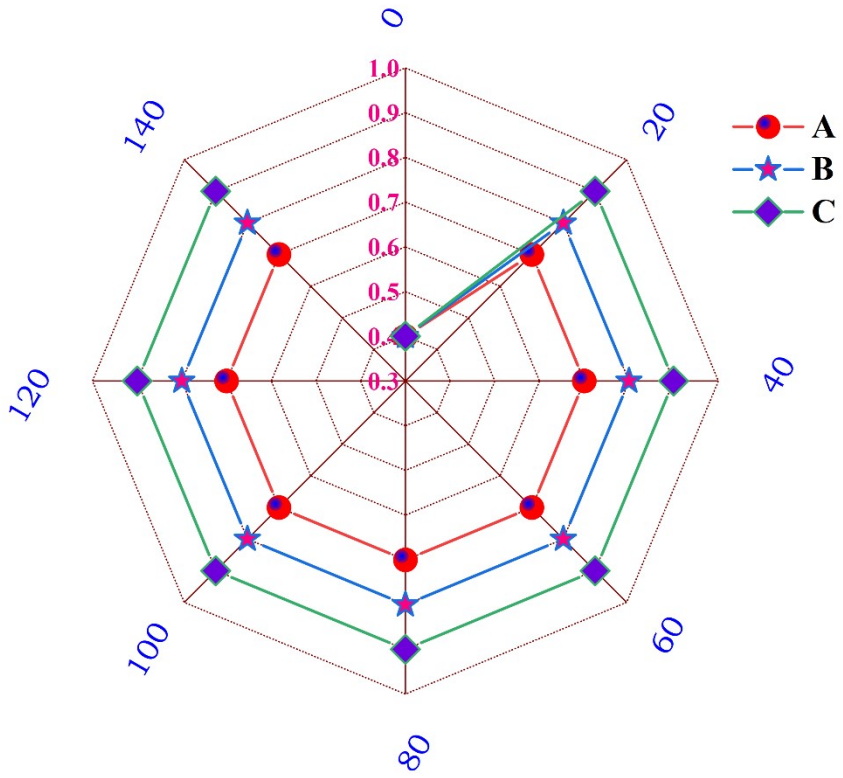

Fig. S15: Response time studies of **DM2-capped ZnO NPs** for quinalphos at various time intervals with varying concentrations of quinalphos (A- 35 nM, B- 70 nM, and C-105 nM).

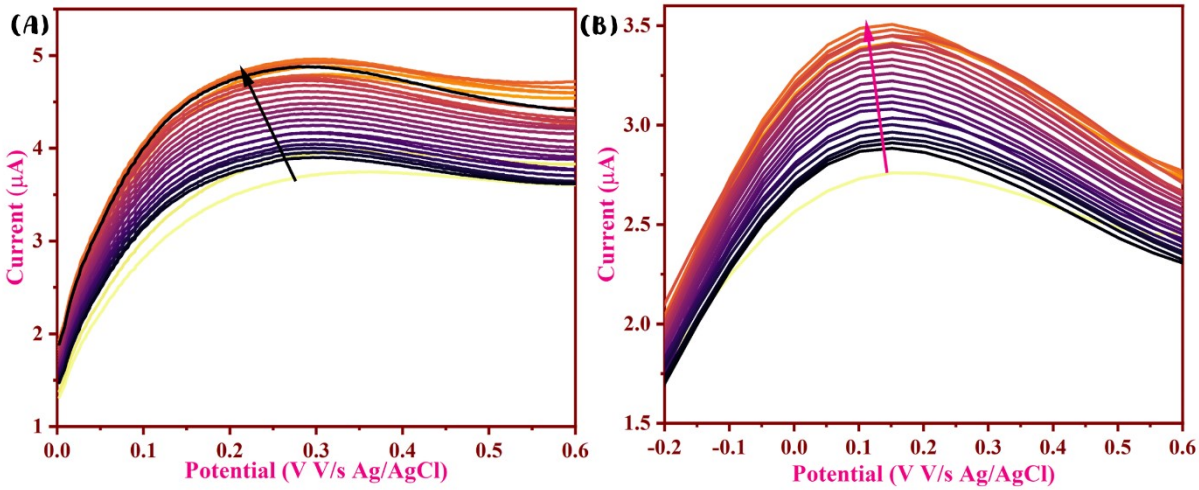

Fig. S16:(A) LSV and (B) DPV plots of **DM2-capped ZnO NPs** upon the successive addition of quinalphos.

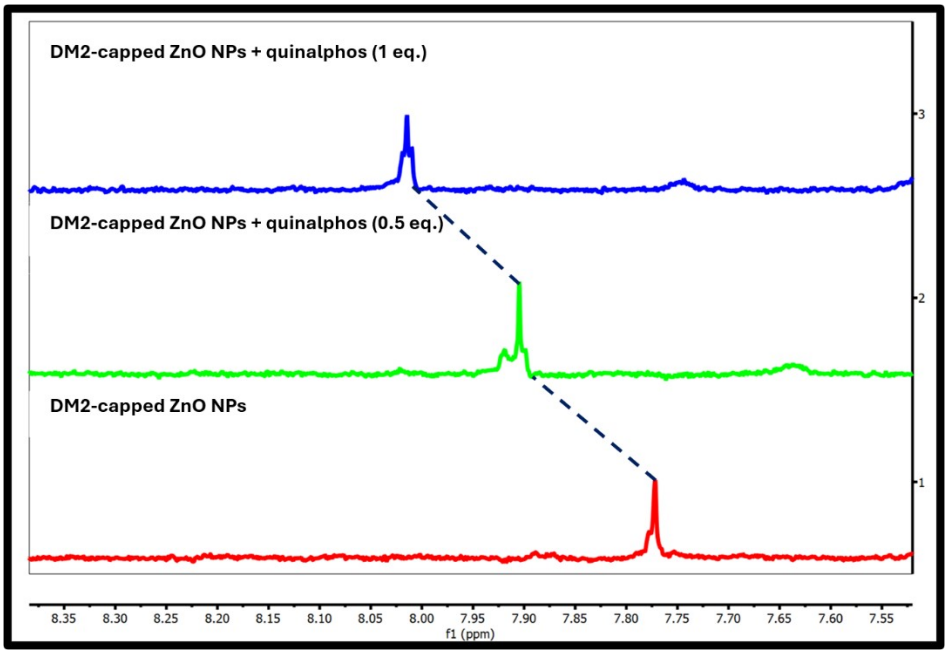

Fig. S17: Shifts in the stacked ^{1}H-NMR spectrum of **DM2-capped ZnO NPs** upon the addition of quinalphos *i.e.,***DM2-capped ZnO NPs+quinalphos** (0.5 *eq.*) and **DM2-capped ZnO NPs+quinalphos** (1 *eq.*).

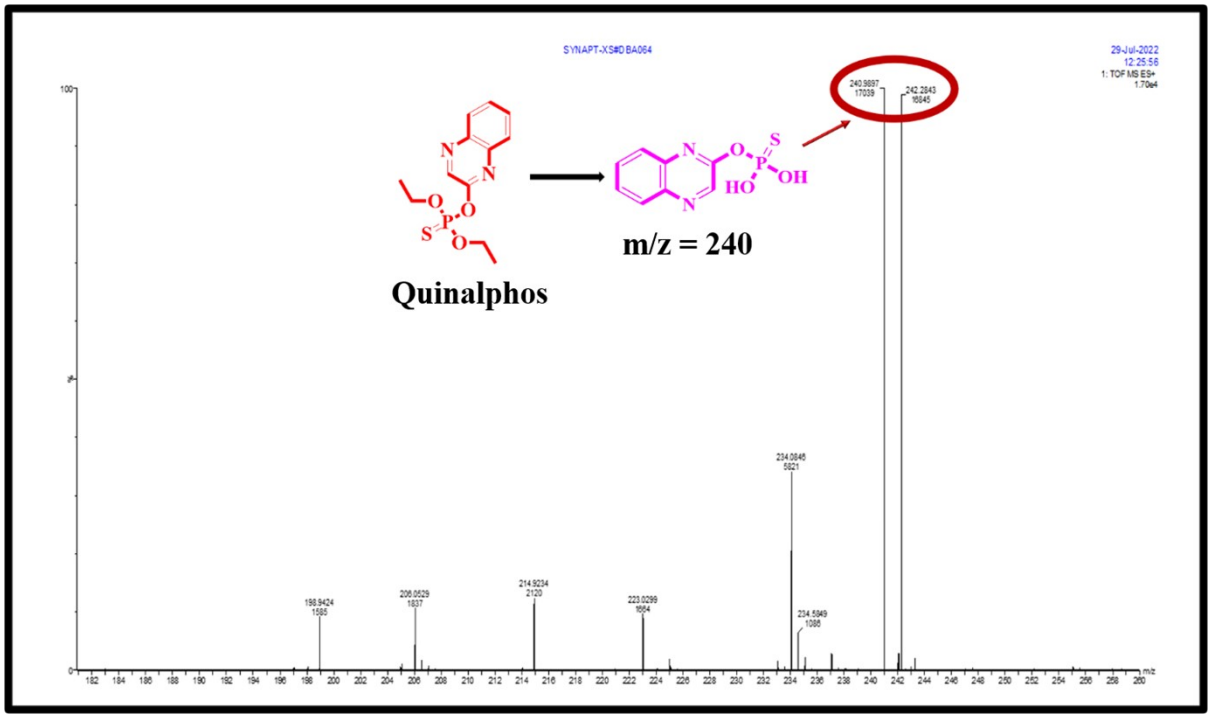

Fig. S18:ESI-MS spectrum of **DM2-capped ZnO NPs+quinalphos** leading to the formation of hydrolyzed product.

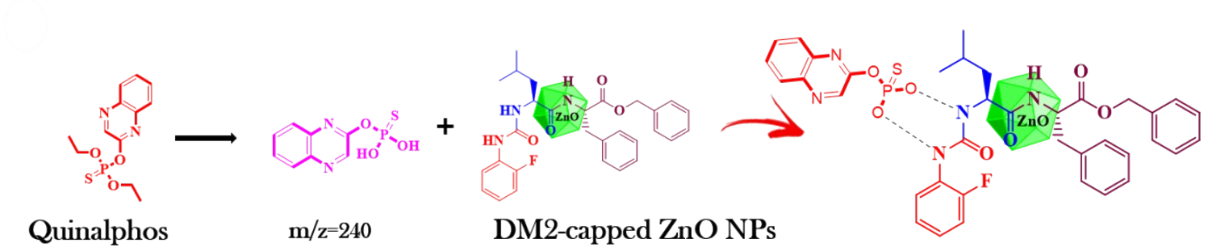

Scheme S1: An efficient route for the detection of quinalphos upon its interaction with **DM2-capped ZnO NPs**.

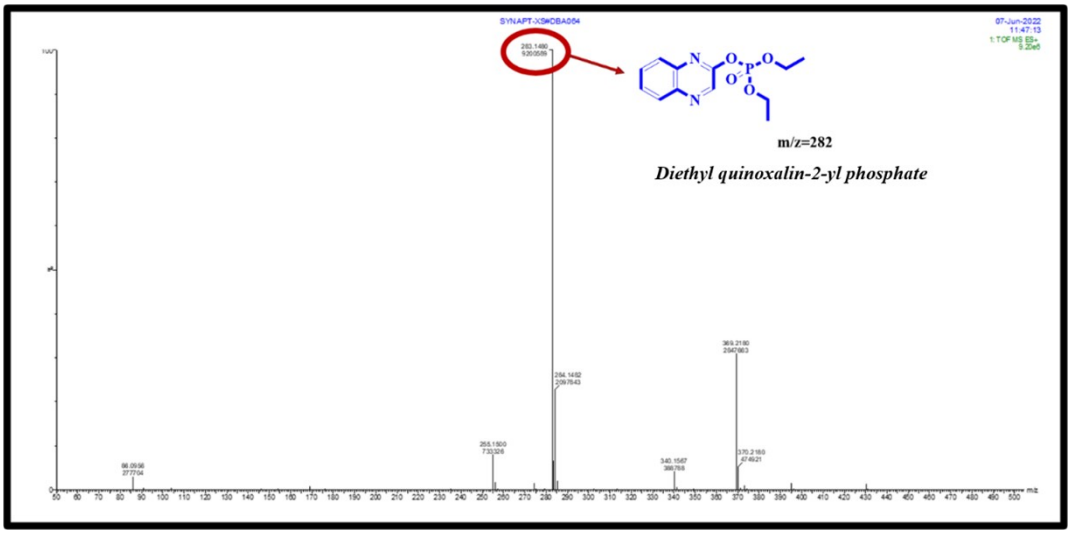

Fig. S19: ESI-MS spectrum of **DM2-capped ZnO NPs+quinalphos** leading to the oxidation of quinalphos, complementing the interaction of **DM2-capped ZnO NPs** with quinalphos.

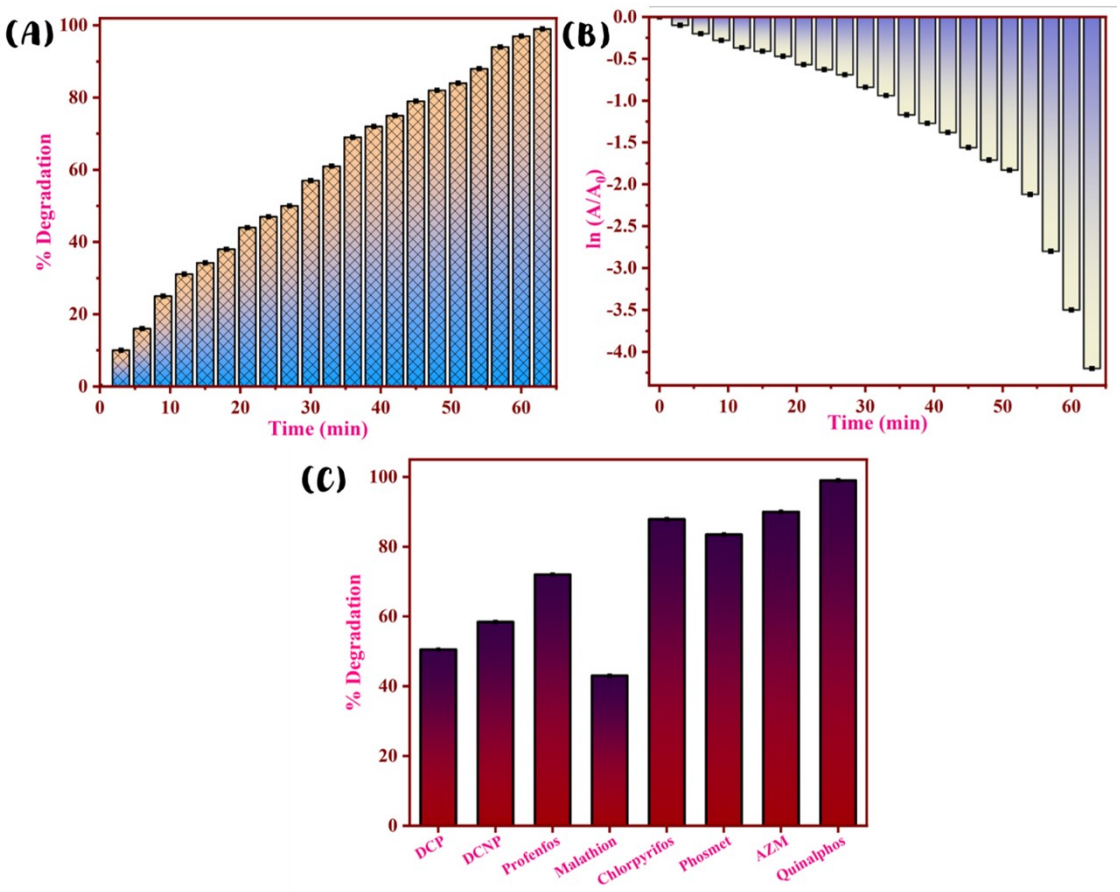

Fig. S20: Photodegradation of quinalphos by **DM2-capped ZnO NPs**. (A) % Degradation of quinalphos and (B) ln (A/A_0) versus time plot showing the pseudo-first-order kinetics; (C) Degradation efficiency of **DM2-capped ZnO NPs** towards the degradation of quinalphos, azinphos-methyl (AZM), phosmet, chlorpyrifos,malathion, profenofos, diethyl cyanophosphate (DCNP), and diethyl chlorophosphate (DCP).

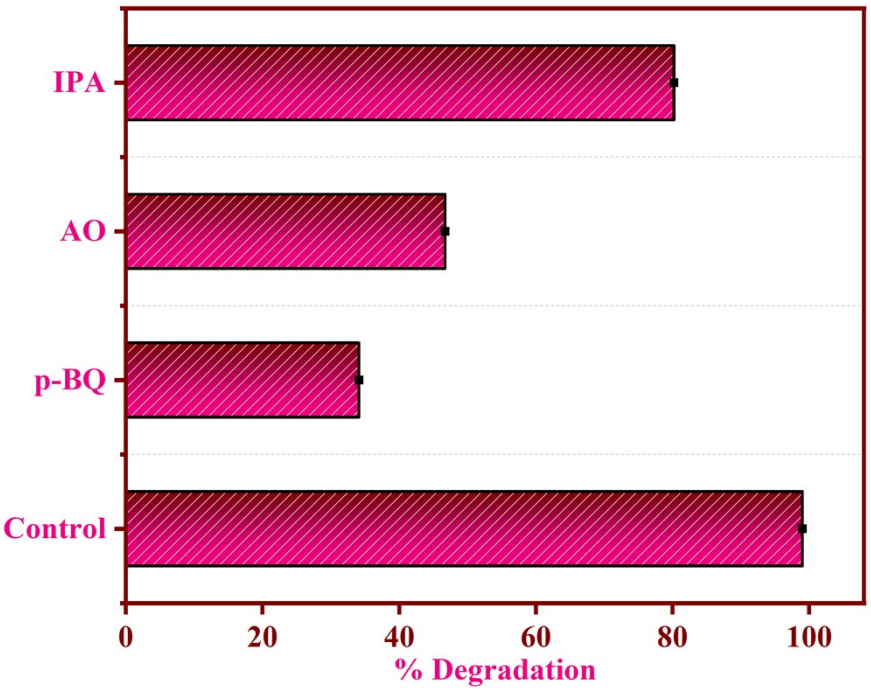

Fig. S21: Radical scavenging experiment.

Fig. S22: ESI-MS spectrum of **DM2-capped ZnO NPs+quinalphos**validating its transformation into *quinoxaline-2-thiol* (m/z=162).

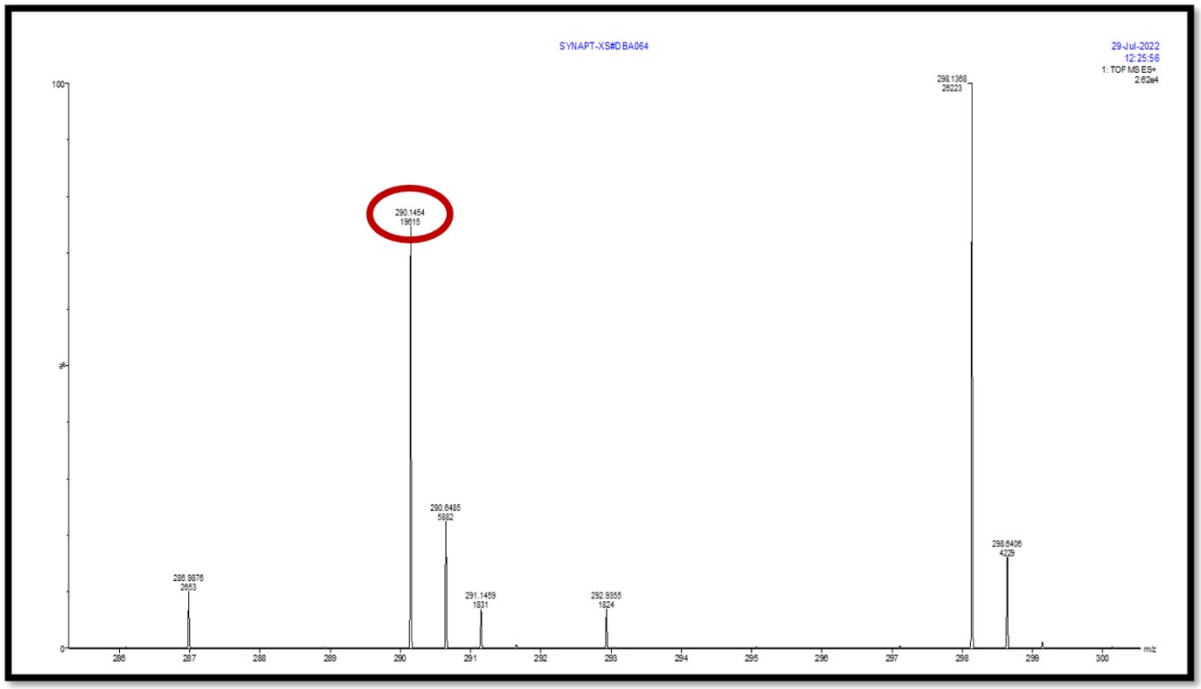

Fig. S23: ESI-MS spectrum of **DM2-capped ZnO NPs+quinalphos**confirming its conversion into *O-ethyl O-({[2-hydroxyamino) phenyl] amino) methyl} hydrogen phosphonothioate* (m/z=290).

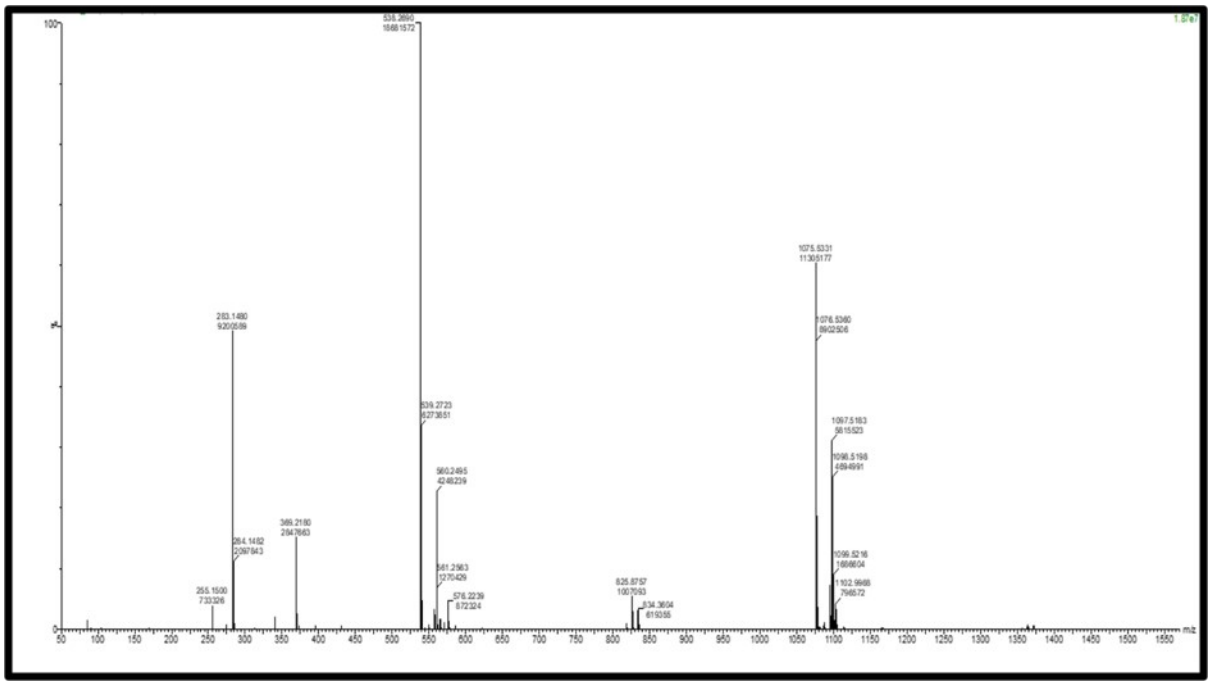

Fig. S24: ESI-MS spectrum showing the absence of peak corresponding to m/z=298 (quinalphos) upon its interaction with **DM2-capped ZnO NPs**.

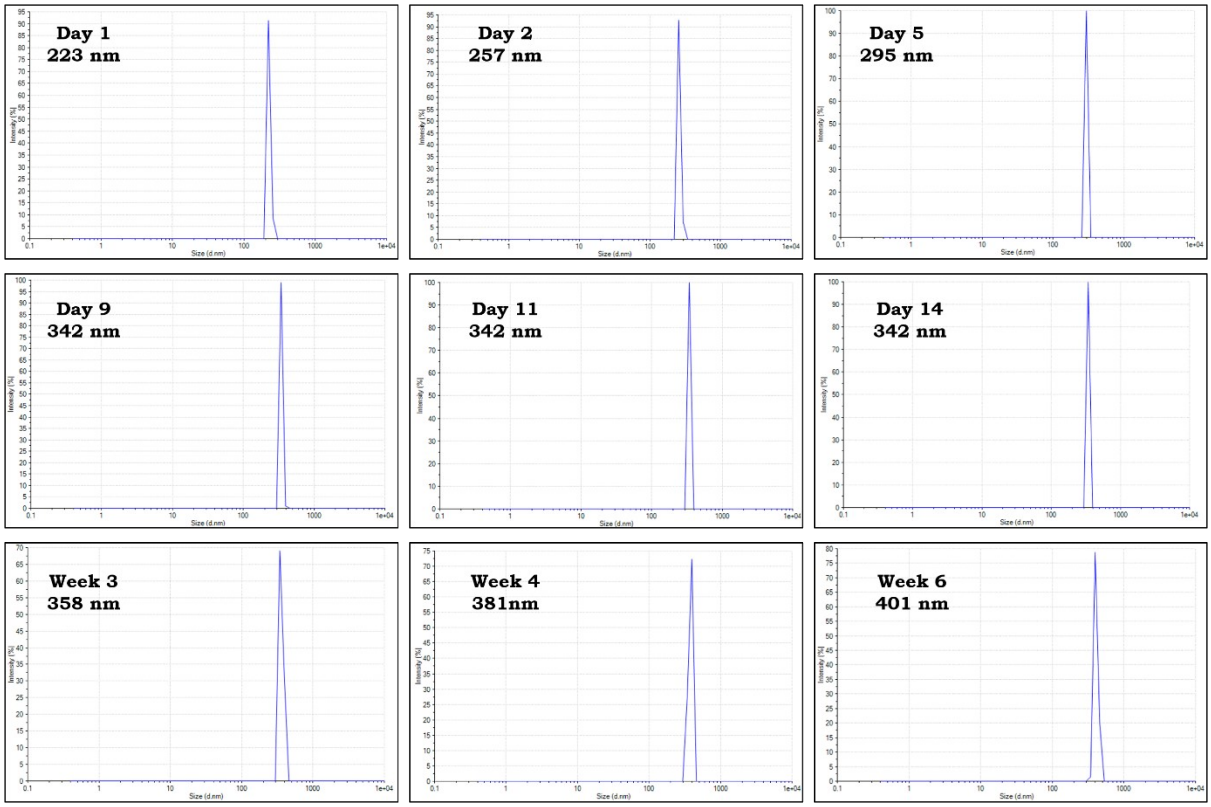

Fig. S25: DLS spectra of QuinoClean (aerospray comprising of 1:1 solution of oleic acid: vegetable oil) showing its stability over 6 weeks at ambient temperature.

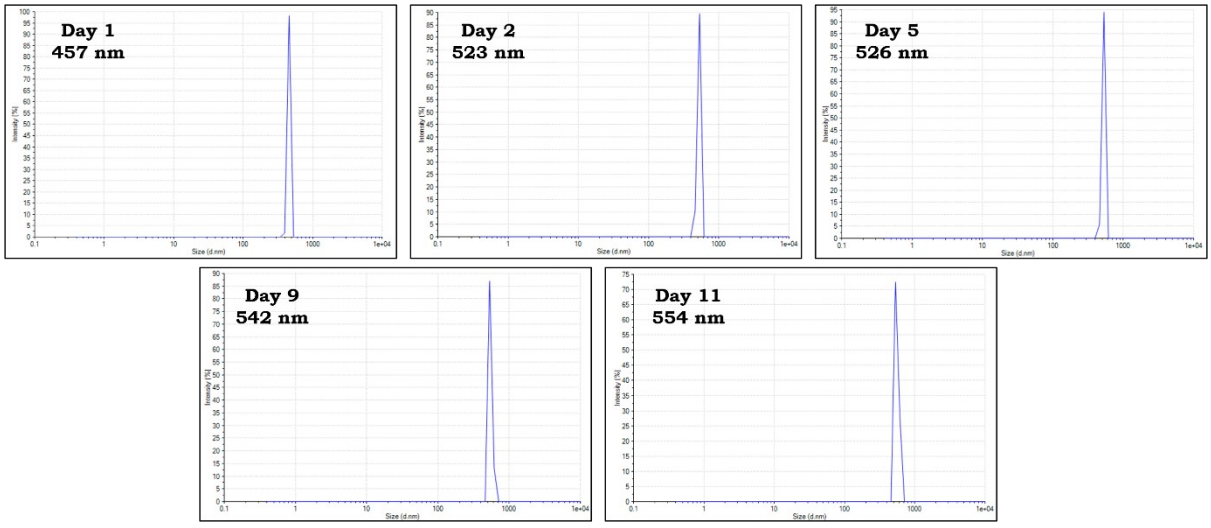

Fig. S26: DLS spectra of 2:1 (oleic acid: vegetable oil) solution for11 days.

Table S1: Comparison of varying amounts of oleic acid and vegetable oil and their corresponding hydrodynamic size.

Sr. No.	Oleic acid	Oil	Size (from DLS)	DLS Spectrum	Stability
1.	1	1	223 nm	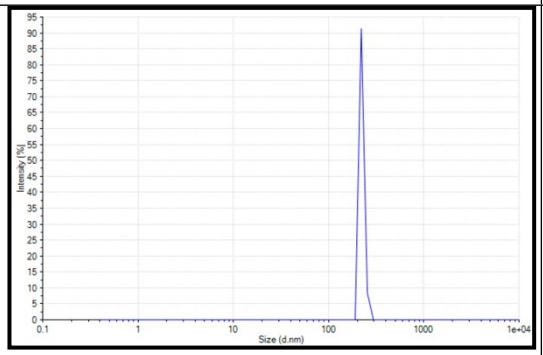	6 Weeks 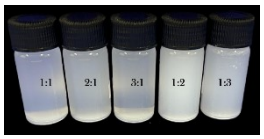
2.	2	1	457 nm	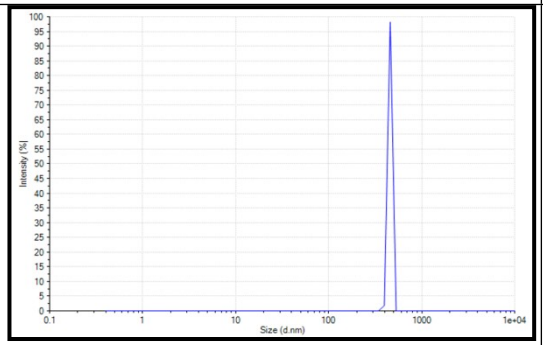	11 days 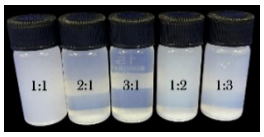
3.	3	1	712 nm	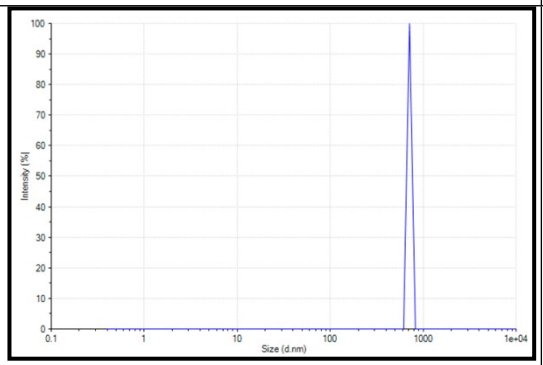	6 days 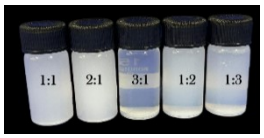
4.	1	2	848 nm	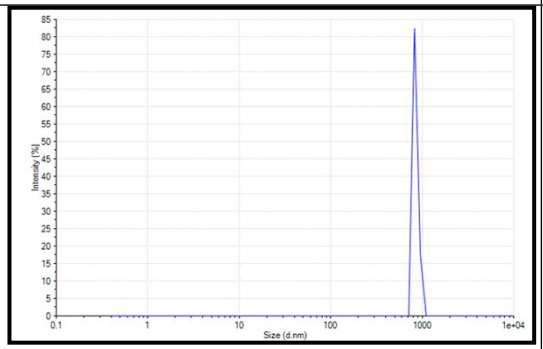	3 days 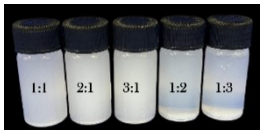

5.	1	3	1281 nm	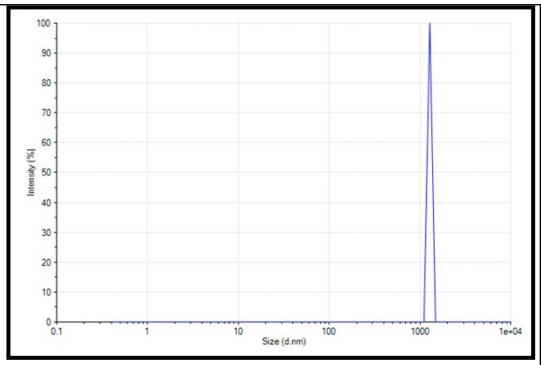	2 days 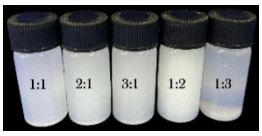

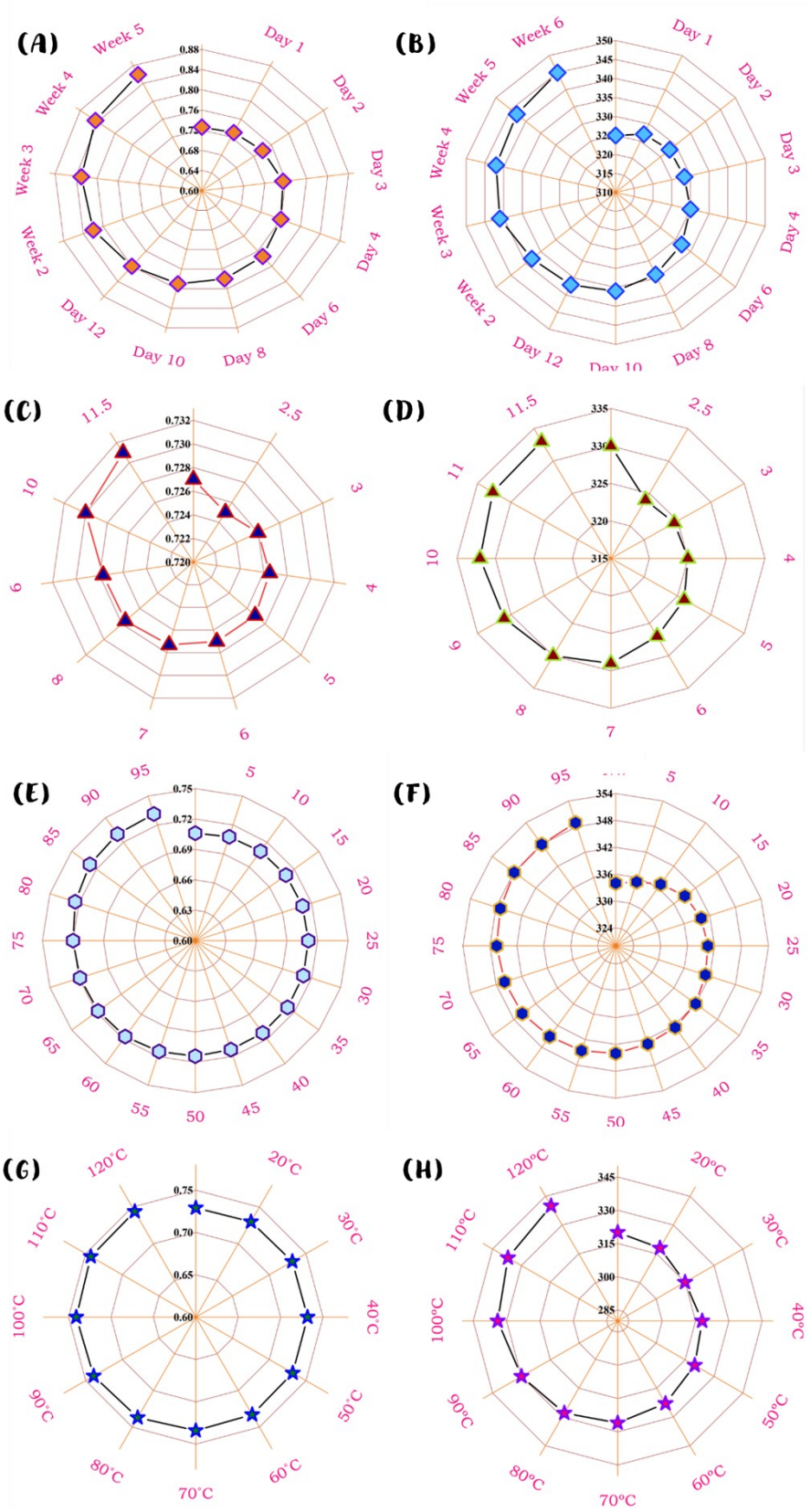

Fig. S27: Changes in the (A, C, E, G) absorbance and (B, D, F, H) FL intensity of **DM2-capped ZnO NPs**-based core@corona formulation (A, B) over 6 weeks; (C, D) upon the addition of 1 mM HCl and 1mM NaOH respectively; (E, F) upon addition of TBA ClO_4^- and (G, H) effect of temperature variation.

Table S2: Comparison table of present work with other analytical techniques.

Sr. No.	Material Used	Technique used	LOD	Detection/ Degradation	Reference
1.	2- amino-4-thiazoleacetic acid anchored AuNPs (ATA-AuNPs)	Colorimetric and spectrophotometric methods	14.37 µg/L	Detection	[1]
2.	GO-ZnO composite	UV irradiation, LC-MS	-	98% Degradation in 45 min	[2]
3.	Azstilbene fluoroprobe	Fluorescence-based detection method	2.0 µM	Detection	[3]
4.	Carbon dots (CDs) from *Tagetes erecta* flower (TEF), named as "TEF-CDs',	Fluorescence assay using CD	1.7 ng/mL	Detection	[4]
5.	Trypsin-encapsulated Au–Ag bimetallic NCs	Fluorescence spectroscopy	0.32 µM	Detection	[5]
6.	Carbon quantum dot integrated metal-organic framework [CD@UiO-66-NH_2-Cu^{2+}]	Fluorescence spectroscopy	0.3 nM	Detection	[6]
7.	PET immunoassay	Photoinduced electron-transfer (PET) immunoassay	0.007 µg/mL	Detection	[7]
8.	*meso*-tetra (4-sulfonatophenyl) porphine ($TPPS_4$)	UV-visible spectroscopy, Fourier transform infrared (FT-IR), and liquid chromatography-	0.01 mg/kg	Detection	[8]

		tandem mass spectrometry (LC-MS/MS)			
9.	Cartridge-based assembly [silica coating of Cu (II)-Au@ONP]	Fluorescence spectroscopy	2.4 nM	Detection	[9]
10.	Sulphur-doped TiO_2 (S–TiO_2)	UV-visible spectroscopy	-	98.09% Degradation	[10]
11.	Aqueous TiO_2 suspension	UV-visible spectroscopy, gas chromatography-mass spectrometry (GC–MS), and ion chromatography (IC)		89% Degradation in 4 h	[11]
12.	Aqueous suspensions of TiO_2	UV-visible spectroscopy and gas chromatography-mass spectrometry (GC–MS)		89.67% degradation in 3 h	[12]
13.	**DM2-capped ZnO NPs-based Type-II heterojunctions [Detection and degradation]**	**Spectroscopic and electrochemical methods**	**2 nM (spectroscopic techniques) and 3 nM (electrochemical techniques)**	**Detection and 99% Degradation in 63 min**	**Present Work**

References

(1) Loganathan, C.; Gowthaman, N. S. K., Microchem. J. 2021, **168**, 106495.

(2) Garg, R.; Gupta, R.; Singh, N.; Bansal, A., Chemosphere 2022, **286**, 131837.

(3) Narayanan, N.; Mandal, A.; Kaushik, P.; Singh, S., Microchem. J. 2022, **175**, 107205.

(4) Ghosh, S.; Gul, A. R.; Park, C. Y.; Kim, M. W.; Xu, P.; Baek, S. H.; Bhamore, J. R.; Kailasa, S. K.; Park, T. J., Chemosphere 2021, **279**, 130515.

(5) Akavaram, S.; Desai, M. L.; Park, T. J.; Murthy, Z. V. P.; Kailsa, S. K., J. Mol. Liq 2021, **327**, 114830.

(6) Bera, M. K.; Behera, L.; Mohapatra, S., Colloids Surf A Physicochem Eng Asp 2021, **624**, 126792.

(7) Liang, Y. F.; Li, J. D.; Fang, R. Y.; Xu, Z. L.; Luo, L.; Chen, Z. J.; Yang, J. Y.; Shen, Y. D.; Ueda, H.; Hammock, B.; Wang, H., Anal Chem 2023, **95**, 12321.

(8) Yang, L.; Han, J.; Liu, W.; Li, J.; Jiang, L., Anal Chem 2015, **87**, 5270.

(9) Rani, R.; Mayank; Thangarasu, P.; Singh, N., ACS Appl Nano Mater 2019, **2**, 1.

(10) Sraw, A.; Kaur, T.; Pandey, Y.; Verma, A.; Sobti, A.; Wanchoo, R. K.; Toor, A. P., Int. J. Environ. Sci. Technol 2020, **17**, 4895.

(11) Kaur, P.; Sud, D., J Mol Catal A Chem 2012, **365**, 32.

(12) Sraw, A.; Toor, A. P.; Wanchoo, R. K., Desalination Water Treat 2016, **57**, 16831.